NUMERICAL INVESTIGATION OF GEOPOLYMER REINFORCED CONCRETE BEAMS UNDER FLEXURAL LOADING USING FINITE ELEMENT ANALYSIS

Yosi N. Wibowo[a], Bambang Piscesa[a*], Yuyun Tajunnisa[a]

***Abstract**: This paper deals with numerical modeling of geopolymer reinforced concrete loaded under flexure using nonlinear finite element analysis. The modeled specimen was obtained from the existing literature and is tested under the four-point bending load. The numerical simulation uses an in-house limited element package called 3D-NLFEA, which utilizes ordinary concrete's multi-surface plasticity model. Since the concrete constitutive model used is for ordinary Portland cement, adjusting the input parameter is required to predict the behavior of geopolymer reinforced concrete. The focus on the discussion was limited to the modeling of the specimen, the moment-curvature result, and the crack pattern between the numerical model and the available experimental test. The simulation found that the predicted moment-curvature relationship using the 3D-NLFEA package was 1.3 to 2.4 % lower than the test result. The crack pattern was controlled by flexure, which was observed in the experimental test and numerical simulation. The predicted crack lengths for modeled beam using 3D-NLFEA were within the minimum and maximum measured crack lengths from the test result.*

Keywords: *Geopolymer concrete, reinforced concrete, plasticity model, finite element analysis, moment-curvature*

INTRODUCTION

The use of silica and alumina sources such as fly ash as the binder component of geopolymer concrete is one alternative to reusing industrial waste [1]. Geopolymer concrete is environmentally friendly and can be made using silica and alumina sources with the alkali activator [2]. Geopolymer is formed from an alkaline activation reaction between sodium hydroxide and sodium silicate solutions with industrial waste such as fly ash, slag, and other pozzolans. The polymerization reaction is very different from the hydration process in Portland cement [3]. This difference in reaction mechanism affects the mechanical properties that lead to the unique behavior of the geopolymer concrete. Therefore, more research on experimental tests and numerical modeling should be conducted [4].

Although the formation phase of geopolymer concrete is different from the ordinary Portland cement concrete, geopolymer concrete can still be considered a quasi-brittle material. The nonlinear stress-strain response observed under different loading axes did represent micro-crack that grows into macro-crack when localized crack in the matrix occurred [5]. From the past research, it can be concluded that the stress-strain behavior of geopolymer concrete is somewhat like concrete made of ordinary Portland cement [6].

Some researchers did some experimental investigations on geopolymer concrete that is used as load-bearing members such as reinforced beams [4, 5, 7], column [8], beam-column joint [9], and composite slab [10]. Uma et al. Uma, et al. [11] performed an experimental and numerical investigation of the flexural response of reinforced geopolymer concrete beams. Uma, et al. [11] use ANSYS to model reinforced concrete with a four-point bending loading scheme. Both experimental data and ANSYS modeling were compared and concluded that there was up to twenty percent difference in the load-carrying capacity of the specimen. Using ABAQUS software, Pham, et al. [12] performed numerical modeling on geopolymer reinforced beams. The moment-curvature response from the numerical analysis shows similarities in the linear elastic and flexural cracking phases. Still, there is a slightly higher bending moment capacity when the steel reinforcing bar yields. From the past numerical simulation, it can be concluded that a proper parameter set for the concrete constitutive model that is calibrated with non-geopolymer concrete (i.e., concrete made with ordinary Portland cement) is required. Therefore, there is a need to study the input parameter for geopolymer concrete when modeled using a constitutive model that applies to standard concrete.

The main objective of this research is to improve the accuracy of the moment-curvature response model of reinforced geopolymer beams using numerical simulation using a nonlinear finite element package called 3D-NLFEA. Two specimen models refer to experimental reinforced concrete conducted by Pham [11], specimen D1 and D2. 3D-NLFEA uses a multi-surface plasticity model [13-17] that can be easily adjusted by providing a new equation or simply changing the parameter in the present equation.

RESEARCH SIGNIFICANCE

This paper investigates the bending moment-curvature behavior of geopolymer reinforced concrete beam using an in-house nonlinear finite element package (3D-NLFEA) that utilizes the multi-surface plasticity model. An adjusted input parameter in the multi-surface plasticity model is proposed to account for improved prediction on the behavior of geopolymer concrete. The numerical simulation concluded that the predicted bending moment-curvature analysis was more accurate and reliable.

METHODOLOGY

The research methodology starts with a brief explanation of the experimental works carried out by [12], which will be investigated using the numerical model proposed in this research. After the details on the specimen geometry are discussed, the proposed modeling approach includes the geometry modeling, meshing, and discussion on the input

[a]Lecturer in the Civil Engineering Department, Institut Teknologi Sepuluh Nopember, ITS Campus, Sukolilo, Surabaya 60111, Indonesia. Corresponding author email address: piscesa@ce.its.ac.id

material properties for the geopolymer concrete, steel platen (support and loading platen), and the steel reinforcement.

A. TEST SPECIMENS AND MATERIAL DATA

Figure 1 shows the geometry details of the beam, cross-sections, supports, and schematic loading, which were experimentally tested by [12]. The beam has a 200 mm width and 300 mm height. The overall beam length is 2,700 mm, and the clear beam span measured from the center-to-center of the support is 2,500 mm. The concrete cover of the beam is 25 mm. The longitudinal reinforcement consisted of two bottom bars and two top bars with 12- and 8-mm diameters. The transverse reinforcement uses a close loop with a 6 mm diameter of rebar and pitch spacing of 80 mm. The load is controlled by displacement control with two loading points apart 900 mm from each other and is located at the mid-span.

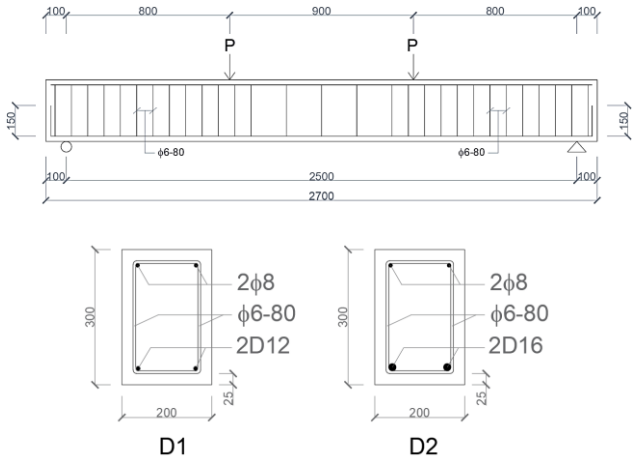

Figure 1 The dimensions and steel reinforcement details of beams

Table 1 shows the geopolymer material properties, while Table 2 shows the rebar material properties. All the material properties are obtained from [11]. From Table 1, the tensile and compressive strengths of the geopolymer concrete are 3.06 and 39.1 MPa, respectively. The geopolymer concrete compressive strength ratio to its tensile strength is 12.77, similar to that of standard strength concrete.

Table 1 Geopolymer concrete material properties [11]

Material Properties	Value
Elastic Modulus (GPa)	32.0
Poisson's ratio	0.2
Compressive strength (MPa)	39.1
Tensile strength (MPa)	3.06

Table 2 Reinforcing bar material properties [11]

Diameter (mm)	Elastic modulus (GPa)	Yield strength f_y (MPa)	Ultimate strength f_u (MPa)
ϕ6	205.5	238.5	322.5
ϕ8	205.5	360.4	524.2
ϕ12	205.5	356.5	527.4
ϕ16	202.5	415.6	552.6

From Table 2, the strain hardening stress from the bars is significantly higher than the yield strength. Therefore, it is wise to consider strain hardening of the reinforcing bar in the numerical modeling. For that purpose, the stress-strain model for the steel reinforcing bar is modeled using a simplified trilinear stress-strain model as shown in Figure 2.

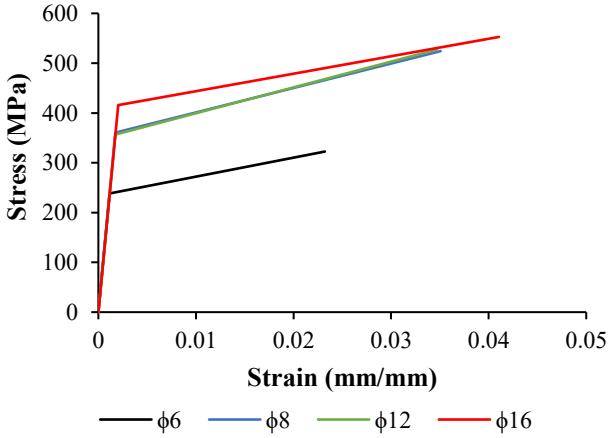

Figure 2 Trilinear stress-strain model of rebar

B. FINITE ELEMENT MODELING, PRE-PROCESSOR, PROCESSOR, AND POST-PROCESSOR

There are three distinguished steps in numerical modeling using finite element analysis: pre-processor, processor, and post-processor. As previously mentioned, this paper uses an in-house 3D-NLFEA finite element package developed by Piscesa, et al. [14]. It should be noted that 3D-NLFEA is a processor. 3D-NLFEA requires input prepared in the pre-processor stage and written output in the .vtk format, which can be read in the post-processor stage using ParaView 5.9.0 [18, 19]. In solving the nonlinear analysis until the equilibrium of the internal and external forces fall below the convergence criteria limit, 3D-NLFEA uses the Tangent Stiffness Like Projection Method (TSLPM, [20]) combined with Process Modification [17, 21, 22] which can accelerate the convergence in the sub-iteration.

In 3D-NLFEA, the concrete is modeled using a multi-surface plasticity model [14], which accounts for modified Menetrey and Willam [23] failure surface for concrete under compression and Rankine [24, 25] failure surface for concrete under tension. For concrete under compression, the flow rule is non-associative, and for concrete under tension, the flow rule is associative. In 3D-NLFEA, the user is only required to fill in the introductory material properties data, and the stress-strain for concrete under compression will be somewhat like [26-28] but applies to the finite element format rather than in empirical formulation.

In the pre-processor stage, all the modeling geometry, boundary conditions, and meshing are done within the open-source platform SALOME 9.3.0 [29]. Figure 3a shows all the solid elements (including geopolymer concrete and steel plates for supports and loading). The steel support and the loading plate are modeled using a steel block size 25 x 200x 200 mm. Figure 3b shows the wire model for the steel reinforcement. In 3D-NLFEA, the solid element is modeled using an eight-noded hexahedral

element with selective integration [30] or the B-Bar element method. The steel reinforcement is modeled using the truss element with the embedded formulation [31, 32].

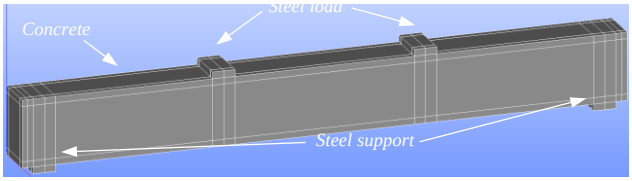

(a) Solid Element

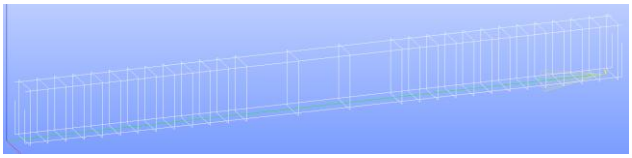

(b) Reinforcement Steel (Wire)

Figure 3 Geometry model

The modeled specimen is loaded with displacement control (monotonic-incremental) static loads. The monotonic load is applied to a line point at the top steel loading platen (as shown in Figure 3). The beam's support is simply supported (left support) where one of the supports is assigned as the hinge, and the other is assigned as a roller (right support). The displacement increment for each time step is set to 0.01 mm. The mesh size of the element is 25 mm.

Table 3 Input parameter for concrete material

Parameters	Value
Concrete Compressive Strength (f_c)	33.16
Modulus of elasticity (E_c)	32000
Poisson's Ratio (ν)	0.2
Density of concrete (ρ)	2556
Internal length scale (L_T)	25
Concrete tensile strength (f_t)	3.06
Out of roundness eccentricity (e)	0.53
Uniaxial axial strain at peak (ε_{cu})	0.0035

Table 4 Input parameter for steel reinforcement

Parameters	Steel Reinforcement		
	ϕ6	ϕ8	ϕ12 & ϕ16
Ultimate strength (f_u, MPa)	322.5	524.2	552.6
Poisson's ratio (ν)	0.30	0.30	0.30
Modulus of elasticity (E_s, GPa)	205.5	205.5	202.5
Plastic strain @f_{y1} (MPa)	0.001	0.002	0.002
Yield strain @f_{y1} (ε_1)	238.5	360.4	415.6
Plastic strain @f_{y2} (MPa)	0.019	0.028	0.041
Yield strain @f_{y2} (ε_2)	322.5	524.2	552.6

3D-NLFEA uses an open-source software GNUplot 5.2 for real-time observation on the load-deformation curve, as shown in Figure 4. In Figure 4, the elastic phase, the initial flexural crack, and yielding of the steel reinforcement were clearly seen.

The output obtained from the numerical modeling is the load (P, in kN) and vertical deformation (Δ) at the loading point. The curvature is then estimated with:

$$\frac{1}{r} = 0.3\frac{8y}{L^2} \quad (1)$$

In Eqn.(1), *1/r* is the curvature, L is the beam span and equal to 2500 mm, and y is the midspan deflection. The bending moment can be computed by:

$$M = Pl_1 \quad (2)$$

In Eqn.(2), l_1 is the length from the support to the first loading platen, measured 800 mm (see Figure 1).

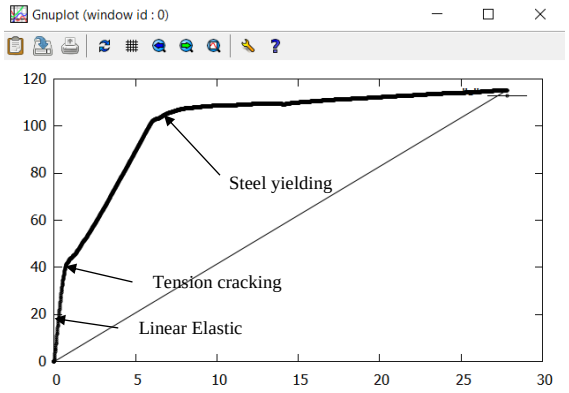

Figure 4 Load-deformation real-time plot using open-source software GNUPlot 5.2.

ANALYSIS AND DISCUSSIONS

Figure 5 shows the moment-curvature relationship for Beam D1 (experimentally tested by [12] and numerical modeling using 3D-NLFEA). The test results show three distinct stages: the linear elastic behavior portion, the onset of localized flexural cracks, and yielding the longitudinal bar [11]. In the elastic zone, the moment-curvature response is linear, which is expected. When the tensile stress in concrete reaches its tensile strength, the concrete cracks and the load-carrying capacity slightly drops. During this phase, a portion of its load is redistributed from the concrete to the longitudinal bars. With the cracked section, the stiffness of the beam is also reduced as the load continues. Once the stress in the longitudinal bar reaches the bar yield strength, an almost flat plateau was observed, and a slight increase in the moment capacity as the curvature increased is observed due to the strain hardening behavior from the steel reinforcement.

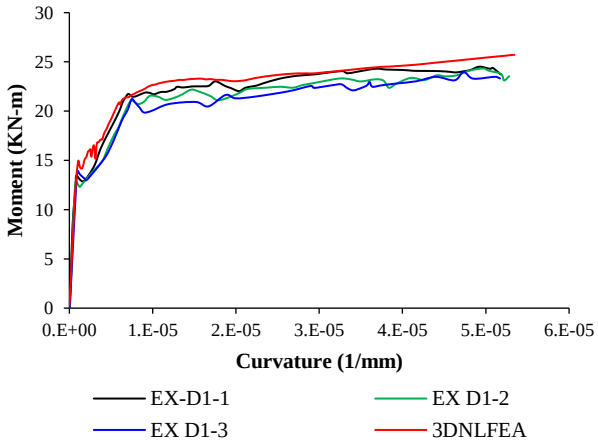

Figure 5 Moment-curvature response of D1 beams

The moment-curvature prediction using 3D-NLFEA shows the excellent prediction for beam D1. As previously mentioned, all three critical points (linear elastic phase, onset of localized flexural crack, and yielding of steel reinforcement) were captured with sufficiently high accuracy—the predicted curvature when the concrete cracks and the bar yields are 1E-6 and 7.1E-6, respectively. The corresponding bending moment is 14.9 kNm and 21.3

kNm, respectively. When yield, the average bending moment capacity from the test results is 21.6 kNm, while the 3D-NLFEA prediction is 21.3 kNm. Therefore, it can be concluded that for beam D1, the 3D-NLFEA prediction was somewhat conservative and is -1.3 % lower than the test result. Pham, et al. [12] also did not carry out numerical simulation for beam D1.

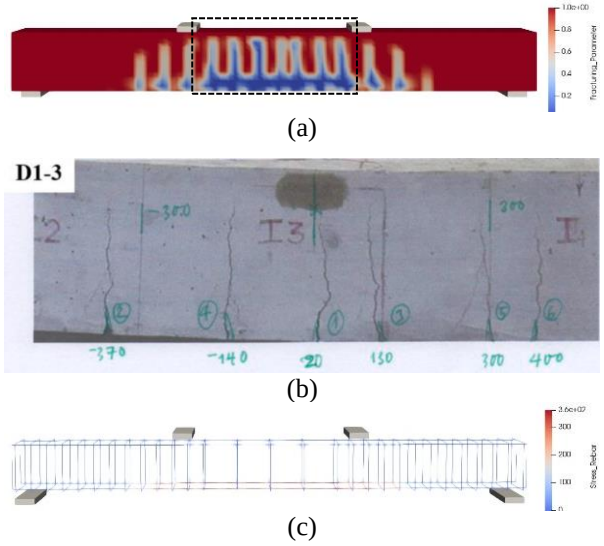

(a)

(b)

(c)

Figure 6 Beam D1 (a) Predicted crack pattern of beam D1 using 3DNLFEA, (b) crack pattern of beam D1-3 [11], (c) stress in the steel reinforcement at yield

Figure 6 shows the predicted crack pattern from the test result [12]. In [12], the crack pattern was closely investigated where both the number of cracks and crack length was measured. The investigation found that crack length for beam D1 was in between 220 and 260 mm (see Figure 6b). On the other hand, the predicted number of cracks for beam D1 using 3D-NLFEA was found to be eight, and the crack length is 250 mm (within the minimum and maximum measured crack length from the test result, see Table 5 for more detail). The vertical cracks in beam D1 indicate that they were primarily caused by bending. Figure 6c shows the bar stresses when it is at yield. At this phase, the beam capacity only increases slightly due to strain hardening from the steel reinforcement. In Figure 6b, it is also seen that the stress in the transverse reinforcement is small. This can be well understood since there is no shear crack occurred in the tested beam.

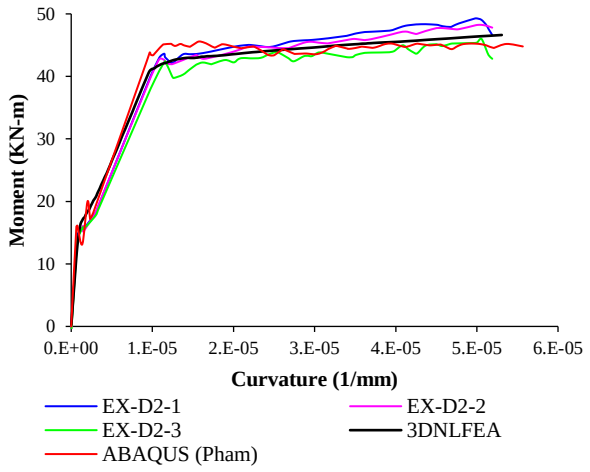

Figure 7 Moment-curvature response of the beam D2

Figure 7 shows the comparison between the test result [12], numerical simulation using ABAQUS [12], and 3D-NLFEA. In Figure 7, it was clearly seen that there existed a double spiked peak for the predicted response using ABAQUS when the concrete cracks. In addition, the numerical simulation carried out by [12] showed higher bending moment capacity when the bar yields. A slight strain hardening response which was existed in the test result was not seen from the ABAQUS simulation.

On the other hand, the predicted response using the 3D-NLFEA package was in good agreement with the test result. At the onset of localized flexural cracking, the predicted bending moment is 16.2 kNm, while the steel yield is 41.1 kNm. From the experimental test [12], the average bending moment at yield is 44.2 kNm. The predicted bending moment at yield for beam D2 is 2.4 % lower than the test result.

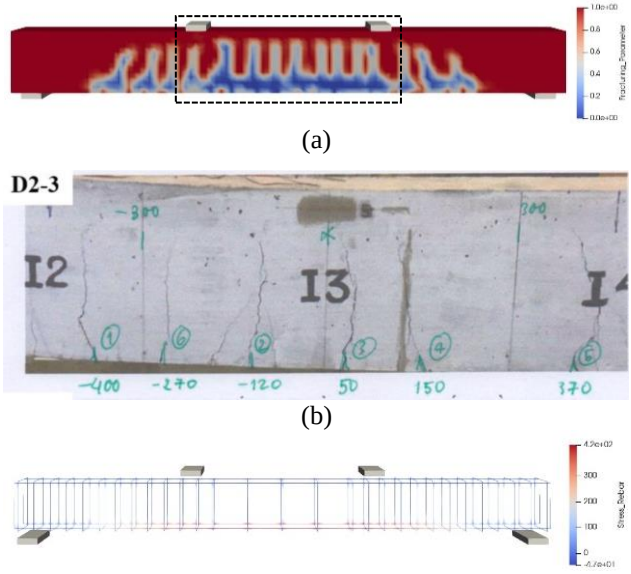

(a)

(b)

(c)

Figure 8 Beam D2 (a) Predicted Crack Pattern of Beam D1 from 3DNLFEA, (b) Crack Pattern of Beam D2-3 [11], (c) Reinforcement Stress at Steel Yielding

Table 5 The number of cracks and their length from the experiment [11] and simulation using 3D-NLFEA

Beam	The number of cracks (Experiment)	The number of cracks (3D-NLFEA)	Maximum distance (Experiment) (mm)	Maximum distance (3D-NLFEA) (mm)
D1-1	4		260	
D1-2	5	8	220	250
D1-3	6		230	
Average crack length:			237	250
D2-1	6		200	
D2-2	5	9	260	240
D2-3	6		220	
Average crack length:			227	240

Table 5 shows the number of cracks and crack length from the experiment [11] and numerically predicted using the 3D-NLFEA package. The experiment shows six vertical cracks with a maximum crack length of 220 mm for beam D2-3 (see Figure 8a and Figure 8b). From the 3D-NLFEA simulation, nine vertical cracks existed for beam D2 with a crack length of 240 mm. The difference in the

visible crack number for beam D2 is more evenly distributed, while for beam D1, it varies, as shown in Table 5. For the bar stresses when the longitudinal bar at yield, similar conclusions were found for beam D2 as in beam D1.

CONCLUSIONS

This paper has presented a numerical investigation of geopolymer reinforced concrete beam tested under four point-load using a 3D-NLFEA finite element package. From the simulation, it can be concluded that the predicted response using 3D-NLFEA was in good agreement with the test result. The linear elastic portion, the onset of localized flexural cracking, and yielding of the steel reinforcement were predicted and measured accurately. The predicted yield bending moment capacity using 3D-NLFEA for beam D1 is -1.3 % lower, and for beam, D2 is 2.4 % higher than the test results.

The number of cracks comparison between the numerical model and the test result may be caused by the selected element size. Theoretically, the smaller the element size, the more flexural cracks formed. Nevertheless, the cracks were dominated by flexure rather than shear. Furthermore, the predicted crack length for beam D1 from the simulation was 250 mm, close to the one measured from the experiment, which is 230 mm. Therefore, it can be concluded that the constitutive model used inside 3D-NLFEA was sufficient to predict the flexure behavior of geopolymer reinforced concrete beams.

REFERENCES

[1] S. Ipek, "Macro and micro characteristics of eco-friendly fly ash-based geopolymer composites made of different types of recycled sand" *Journal of Building Engineering,* vol. 52, p. 104431, 2022.

[2] J. Davidovits, "Geopolymer cement," *A review. Geopolymer Institute, Technical papers,* vol. 21, pp. 1-11, 2013.

[3] A. M. Fernandez-Jimenez, A. Palomo, and C. Lopez-Hombrados, "Engineering properties of alkali-activated fly ash concrete," *ACI Materials Journal,* vol. 103, no. 2, p. 106, 2006.

[4] K. T. Nguyen, T. A. Le, and K. Lee, "Experimental study on flexural strength of reinforced geopolymer concrete beams," *International Journal of Civil and Environmental Engineering,* vol. 10, no. 4, pp. 516-520, 2016.

[5] K. T. Nguyen, N. Ahn, T. A. Le, and K. Lee, "Theoretical and experimental study on mechanical properties and flexural strength of fly ash-geopolymer concrete," *Construction and Building Materials,* vol. 106, pp. 65-77, 2016.

[6] D. Hardjito and B. V. Rangan, "Development and properties of low-calcium fly ash-based geopolymer concrete," 2005.

[7] Y. Du, J. Wang, C. Shi, H.-J. Hwang, and N. Li, "Flexural behavior of alkali-activated slag-based concrete beams," *Engineering Structures,* vol. 229, p. 111644, 2021.

[8] P. Saranya, P. Nagarajan, and A. Shashikala, "Behaviour of GGBS-dolomite geopolymer concrete short column under axial loading," *Journal of Building Engineering,* vol. 30, p. 101232, 2020.

[9] P. Saranya, P. Nagarajan, and A. Shashikala, "Behaviour of GGBS-dolomite geopolymer concrete beam-column joints under monotonic loading," in *Structures*, 2020, vol. 25: Elsevier, pp. 47-55.

[10] A. Ataei, M. A. Bradford, and X. Liu, "Experimental study of composite beams having a precast geopolymer concrete slab and deconstructable bolted shear connectors," *Engineering Structures,* vol. 114, pp. 1-13, 2016.

[11] K. Uma, R. Anuradha, and R. Venkatasubramani, "Experimental investigation and analytical modeling of reinforced geopolymer concrete beam," *International Journal of Civil & Structural Engineering,* vol. 2, no. 3, pp. 817-827, 2012.

[12] D. Q. Pham, T. N. Nguyen, S. T. Le, T. T. Pham, and T. D. Ngo, "The structural behaviours of steel reinforced geopolymer concrete beams: An experimental and numerical investigation," in *Structures*, 2021, vol. 33: Elsevier, pp. 567-580.

[13] B. Piscesa, M. Attard, A. Samani, and S. Tangaramvong, "Plasticity constitutive model for stress-strain relationship of confined concrete," *ACI Structural Journal,* vol. 114, no. 2, p. 361, 2017.

[14] B. Piscesa, M. M. Attard, D. Prasetya, and A. K. Samani, "Modeling cover spalling behavior in high strength reinforced concrete columns using a plasticity-fracture model," *Engineering Structures,* vol. 196, p. 109336, 2019.

[15] B. Piscesa, M. M. Attard, and A. K. Samani, "A lateral strain plasticity model for FRP confined concrete," *Composite Structures,* vol. 158, pp. 160-174, 2016.

[16] B. Piscesa, M. M. Attard, and A. K. Samani, "Three-dimensional finite element analysis of circular reinforced concrete column confined with FRP using plasticity model," *Procedia Engineering,* vol. 171, pp. 847-856, 2017.

[17] B. Piscesa, M. M. Attard, and A. K. Samani, "3D Finite element modeling of circular reinforced concrete columns confined with FRP using a plasticity based formulation," *Composite Structures,* vol. 194, pp. 478-493, 2018.

[18] J. Ahrens, B. Geveci, C. Law, C. Hansen, and C. Johnson, "36-ParaView: An end-user tool for large-data visualization," *The Visualization Handbook,* p. 717, 2005.

[19] U. Ayachit, *The paraview guide: a parallel visualization application*. Kitware, Inc., United States, 2015.

[20] B. Piscesa, "Modeling Confined Concrete Using Plasticity Formulation," PhD. Thesis, School of Civil and Environmental Engineering, The University of New South Wales, Sydney, Australia, 2018.

[21] R. Lawther, "Modification of iterative processes for improved convergence characteristics," *International Journal for Numerical Methods in Engineering,* vol. 15, no. 8, pp. 1149-1159, 1980.

[22] D. J. O'Shea, M. M. Attard, D. C. Kellermann, and C. Sansour, "Nonlinear finite element formulation based on invariant-free hyperelasticity for orthotropic materials," *International Journal of Solids and Structures,* vol. 185, pp. 191-201, 2020.

[23] P. Menetrey and K. Willam, "Triaxial failure criterion for concrete and its generalization," *ACI structural Journal*, vol. 92, no. 3, 1995.
[24] W.-F. Chen, *Plasticity in reinforced concrete*. J. Ross Publishing, 2007.
[25] W.-F. Chen and D.-J. Han, *Plasticity for structural engineers*. J. Ross Publishing, 2007.
[26] M. Attard and S. Setunge, "Stress-strain relationship of confined and unconfined concrete," *ACI Materials Journal*, vol. 93, no. 5, 1996.
[27] A. Samani and M. Attard, "A stress-strain model for uniaxial and confined concrete under compression," *Engineering Structures*, vol. 41, pp. 335-349, August 2012, doi: http://dx.doi.org/10.1016/j.engstruct.2012.03.027.
[28] A. K. Samani and M. M. Attard, "Lateral strain model for concrete under compression," *ACI Structural Journal*, vol. 111, no. 1-6, 2014.
[29] *SALOME - The Open source integration platform for numerical simulation. http://www.salome-platform.org/*. (2019). [Online]. Available: http://www.salome-platform.org/
[30] T. J. Hughes, *The finite element method: linear static and dynamic finite element analysis*. Courier Corporation, 2012.
[31] A. Ranjbaran, "Embedding of reinforcements in reinforced concrete elements implemented in DENA," *Computers and Structures*, vol. 40, no. 4, pp. 925-930, 1991.
[32] A. Ranjbaran, "Mathematical formulation of embedded reinforcements in 3D brick elements," *Communications In Numerical Methods In Engineering*, vol. 12, no. 12, pp. 897-903, 1996.